SUPPLEMENTARY MATERIALS

Supplementary Methods

Mice. All animal procedures were approved by the Institutional Animal Care and Use Committee at UT Southwestern Medical Center. Tg(Cx30.2-MerCreMer) mice were generated as previously described(11). Multiple founders were identified and characterized, and a single representative line was maintained. Rosa26$^{LacZ/LacZ}$ (#003309), Rosa26$^{DTA/DTA}$ (#009669), and Rosa26$^{tdTomato/tdTomato}$ (#007914) mice were purchased from Jackson Labs and maintained on a C57BL6 background.

Tamoxifen (T5648; Sigma) was dissolved in a mixture of sesame oil and ethanol (sesame oil to ethanol: 9:1) to a concentration of 50-100 mg/mL and stored at -20°C. Initial tamoxifen dosing studies were performed in Tg(Cx30.2-MerCreMer); Rosa26$^{LacZ/+}$ animals to determine the extent of labeling. The dosing regimens were based on previously published studies in which the Myh6-MerCreMer allele was used to maximally label cardiomyocytes in neonates(3) and adults(34), acknowledging that our studies use a different Cre driver line that is more anatomically restricted. We extrapolated from the adult dosing regimen to juveniles but found that injections after the fifth day (P19) would often result in extravasation of tamoxifen from the abdominal cavity. We did not choose to pursue a multi-day injection regimen in neonates to minimize cannibalization by the mother (our unpublished observations). Adult Tg(Cx30.2-MerCreMer)/+; Rosa26$^{DTA/LacZ}$ mice were injected intraperitoneally with 1 mg tamoxifen per day from P42 to P48; juvenile mice were similarly injected from P14 to P19. Neonatal Tg(Cx30.2-MerCreMer)/+; Rosa26$^{DTA/LacZ}$, Tg(Cx30.2-MerCreMer)/+; Rosa26$^{lacZ/+}$, Tg(Cx30.2-MerCreMer)/+; Rosa26$^{DTA/tdTomato}$, and Tg(Cx30.2-MerCreMer)/+; Rosa26$^{tdTomato/+}$ mice were injected subcutaneously with a single dose of 1 mg tamoxifen at P0. Throughout the manuscript, we have used the following genotype labeling conventions unless otherwise specified: control: Rosa26$^{DTA/LacZ}$, iAVB or iAVB/LacZ: Tg(Cx30.2-MerCreMer)/+; Rosa26$^{DTA/LacZ}$, AVCS-iLacZ: Tg(Cx30.2-MerCreMer)/+; Rosa26$^{LacZ/+}$, AVCS-iCre: Tg(Cx30.2-MerCreMer)/+; Rosa26$^{tdTomato/+}$.

Sample sizes were estimated based on prior experience, and no initial power calculation was performed. Animals were not formally randomized, but all animals received equal amounts of tamoxifen

and were used for subsequent studies if they survived the induction period. The experimenter was blinded to genotyping information until the first EKG taken at p7 for neonates and before the first tamoxifen injection for juveniles at p14 and adults at p42. Unless otherwise stated, both males and females were used in all experiments and compared with age-matched controls.

Antibodies. The following antibodies were used: anti-HCN4 guinea pig polyclonal antibody, 1:200 (#AGP-004, Alomone Labs, Jerusalem, Israel); anti-HCN4 rabbit polyclonal antibody, 1:200 (#APC-052, Alomone Labs, Jerusalem, Israel); anti-HCN4 mouse antibody, 1:200 (#75-150, Antibodies Incorporated-NeuroMab); anti-α-actinin mouse monoclonal antibody, 1:400 (#A7811, MilliporeSigma); anti-Histone H3 (phosphor S10) rabbit polyclonal antibody, 1:200 (#ab5176, Abcam); anti-Nppa Rabbit polyclonal, 1:200 (#AP8534a, Abgent); anti-Myl2 Rabbit polyclonal antibody, 1:200 (#50-559-132, Fisher Scientific); Connexin 30.2 rabbit polyclonal antibody, 1:200 (ThemoScientific/Life Techonogies); Anti-Connexin-40, 1:200 (#ACC-205, Alomone Labs, Jerusalem, Israel); Anti-Connexin-45, 1:200 (#ACC-207, Alomone Labs, Jerusalem, Israel); Caspase-3 (Asp175) (5A1E) Rabbit mAb, 1:200 (#9664, Cell Signaling Technology); Alexa Fluor 488 Goat anti-chicken IgY H&L, 1:400 (#ab150169, Abcam); Alexa Fluor 488 Goat anti-Rabbit IgG (H+L) Antibody, 1:400 (# A11034, Invitrogen); Alexa Fluor 488 Goat anti-mouse IgG (H+L) Antibody, 1:400, (# A11001, Invitrogen); Alexa Fluor 555 Goat anti-Mouse IgG (H+L), 1:400 (# A21422, Invitrogen); Alexa Fluor 488 Goat anti-guinea pig IgG (H+L), 1:400 (# A11073, Invitrogen).

Histology. Adult mice were euthanized with CO_2, and the hearts were collected. For paraffin-embedded sections, Tg(Cx30.2-MerCreMer)/+; Rosa26$^{DTA/LacZ}$ and Tg(Cx30.2-MerCreMer)/+; Rosa26$^{LacZ/+}$ hearts were harvested and fixed with 0.2% glutaraldehyde for one hour at 4°C and washed with washing buffer with 0.01% deoxycholic acid (#D2510, Millipore-Sigma), 0.02% NP-40 (#56741, Millipore-Sigma) in PBS for 10 minutes twice. The hearts were then incubated in X-gal staining buffer with 2mM Magnesium chloride (M13448, Fisher Scientific, Fair Lawn, New Jersey), 5mM Potassium ferricyanide, 5mM Potassium ferrocyanide (#P3289, MilliporeMilliporeSigma), 0.01% deoxycholic acid, 0.02% NP-40 and 1mg/ml X-gal (B1690, Thermal Fisher Scientific, Eugene, OR) in PBS at room

temperature overnight. Whole mount pictures were taken with a dissection microscope, and the hearts were then post-fixed in neutral formalin overnight and sent to UTSW Molecular Pathology Core Facility for paraffin bedding and sectioning. The paraffin blocks were conventionally sectioned from the front of the heart according to the well-established technique in the pathology core facility. H&E and trichrome staining of paraffin sections was performed according to established staining protocols at the UTSW Molecular Pathology Core Facility. Since the atrioventricular node lies at the lower part of atrioventricular septum, the heart sections were sequentially collected when both mitral valve and tricuspid valve were present in the field, and sectioning was stopped after exhausting both mitral and tricuspid valves. To identify sections through the AVCS, an initial survey was performed with H&E staining to identify the AVCS using anatomical landmarks. Then, MTC collagen staining was used to confirm the anatomical location of the AVCS, and matching sections were identified for littermate controls. For sections that were stained with X-gal, nuclear-fast red (NFR) was used as a counterstain for better visualization of X-gal$^+$ cells.

For cryo-sections, Tg(Cx30.2-MerCreMer)/+; Rosa26$^{DTA/tdTomato}$, and Tg(Cx30.2-MerCreMer)/+; Rosa26$^{tdTomato/+}$ hearts were fixed with 4% paraformaldehyde (PFA) for one hour at 4°C, then incubated in 30% sucrose/PBS at 4°C overnight and cryo-embedded in Tissue Freezing Medium (TFM) (#72592, Electron Microscopy Sciences). Tg(Cx30.2-MerCreMer)/+; Rosa26$^{DTA/LacZ}$, Tg(Cx30.2-MerCreMer)/+; Rosa26$^{lacZ/+}$ hearts were directly cryo-embedded in TFM. All embedded hearts were placed in the four chamber orientation and snap-frozen in isopentane bath (2-Methylbutane, #M32631, Millipore Sigma, St. Louis, MO) heat extractant super-cooled to -155°C in liquid nitrogen or directly on dry ice. Resulting blocks were stored at -80°C prior to sectioning. Eight-micron sections were prepared on a Leica CM3050S cryostat. Cryo-embedded hearts were sectioned from the back of the heart. The sectioning technique was adjusted to the age of the hearts. Since the AVN and AVCS lie deep within the lower part of the atrioventricular septum near the septal leaflet of the tricuspid valve, the septal leaflets were used as a prominent landmark for the AVN in adult hearts. For younger hearts at p2, it was safe to sequentially collect sections when the chamber of right atrium was present in the field. For the adult

heart, the sections were collected when the septal leaflet was emerging in the field. The sections were also checked under the microscope for the progress of chambers, valves, subtle orientations of the heart, and appearance of the compact AVN. Sectioning of the AVN was halted when both tricuspid and mitral valves were exhausted. The cell-type identity was confirmed by immunostaining for specific positive (Hcn4) and negative (Nppa/Myl2) markers of the AVCS, and matching sections were identified for littermate controls. Trichrome staining of cryosections was performed with the One-step Trichrome Blue/Red Stain Kit (#KTTRBPT, American MasterTech Scientific). Acetylcholinesterase activity staining was performed with modifications to previously published protocols(35, 36). Briefly, air-dried sections were fixed in 0.2% glutaraldehyde/PBS for 10 min at room temperature, then washed thoroughly in two changes of distilled water for 2 min each. The sections were then incubated at 37°C overnight in acetylthiocholine staining buffer which was made of 0.5mg/ml Acetylthiocholine iodide (#A5715, Sigma), 0.06N sodium acetate (#110191, Sigma), 0.1N acetic acid, 0.1M sodium citrate (#SX0445-1, VWR), 30mM cupric sulfate (#209198, Sigma), 4mM iso-OMPA (#T1505, Sigma), and 0.5M potassium ferricyanide. The slides were rinsed in distilled water and counterstained in freshly filtered Harris hematoxylin according to standard protocols.

Immunostaining. Frozen slides were air dried for 15~20 minutes at room temperature, fixed with 4% PFA in PBS for 20 minutes on ice, and washed with three changes of PBS. Fixed slides were then permeabilized with 0.3% Triton-X100 in PBS for 20 minutes at room temperature and rinsed with three changes of PBS. They were subsequently blocked with Universal Blocking buffer for 10 minutes at room temperature or M.O.M blocking buffer for 1 hour at room temperature, followed by 5% goat serum in M.O.M protein diluent. Primary antibodies were diluted in the appropriate diluent and incubated overnight at 4°C. Stained sections were washed three times with PBS buffer and incubated with respective secondary antibodies for 1 hour at room temperature. After washing, the sections were mounted with Vectashield Mounting Medium with DAPI (H-1200, Vector Labs) for microscopy. Images were taken using a Zeiss LSM510 confocal, Nikon A1R confocal, or epifluorescence microscope. To identify sections through the AVCS, an initial survey was performed with AChase staining on

cryosections to localize components of the cardiac conduction system. Then, a second survey was done with H&E staining to identify the AVCS using anatomical landmarks. Finally, the cell-type identity was confirmed by immunostaining for specific positive (Hcn4) and negative (Nppa/Myl2) markers of the AVCS, and matching sections were identified for littermate controls.

Microscopy and Image analysis. Review and photography of histologic preparations were carried out on a Leica DM2000 photomicroscope equipped with bright-field and epifluorescence illumination. Photomicrographs were obtained with an Optronics Microfire digital CCD color camera interfaced with a Macintosh G4 computer, captured using PictureFrame 2.0 acquisition software (Optronics Inc. Goleta, CA, USA), and processed with Adobe Photoshop CS2. The fibrosis of the atrioventricular node was analyzed with Fiji. Briefly, the Trichrome stained slides were color deconvoluted with Masson Trichrome vector, and the fibrosis area was measured after adjusting the threshold. Fibrosis area was quantified as the fraction of total atrioventricular node area. Quantification of pH3-positive cells were conducted as follows. The pictures of heart immunofluorescence staining sections were captured at z-sections with 0.1-µm intervals using the laser filters of 408nm, 488nm, 555nm and 647nm by Nikon A1R+ scanning confocal system with 10X and 20X objectives. The pinholes of all four channels were set at 1.2 Airy units. The laser power for the DAPI, HCN4, and α-actintin channels were set at 5, while laser power for the pH3 channel was set at 1. The atrioventricular node area was anatomically marked by HCN4 positivity. The nuclei in the Region of Interest (ROI) of the atrioventricular node and HCN4 drop outs were processed and counted by the function "Object count" of NIS-Elements Advanced Research Version 4.50. pH3-positive cells were first located on Maximum Projection image and then carefully checked for co-localization with DAPI nuclear staining, and AVN marker HCN4 positive cells, or cardiomyocyte marker α-actintin positive cells at the window of slices view. pH3 positive cells were calculated by the ratio of positive cell number to the nuclei. HCN4 drop out was calculated by the ratio of HCN4 positive area to the area of atrioventricular node.

Echocardiography. Cardiac function was evaluated by two-dimensional transthoracic echocardiography on conscious mice using the Visual Sonics Vevo 2100 (Visualsonic, Canada),

equipped with a 40MHz mouse ultrasound probe. The heart was imaged in a parasternal short-axis view at the level of the papillary muscles to record M-mode measurements and to determine heart rate, wall thickness, and end-diastolic and end-systolic dimensions. Fractional shortening was calculated based on end diastolic and end systolic dimensions obtained from M-mode ultrasound.

ECG analysis. All ECGs were obtained either by BioAmp connected to a Powerlab (ADInstruments, CO, U.S.A) or with a Vevo 2100 at the time of echocardiography. ECG signals were analyzed with LabChart8 (ADInstruments, CO, U.S.A). Mice were anesthetized with 2% isofluorane in 200 mL/min oxygen, and subcutaneous leads were placed in the conventional lead II position. Since the PR intervals of neonatal mice shorten as they grow, normal PR intervals were obtained at p2, p4, p7, p14, p21, p28, p35 and adults. The normal range of PR intervals were set as Mean ± 2 Standard Deviation:

	P7	P14	P21	P28
Average PR interval (ms)	51	39	38	37
Mean ± 2SD (ms)	38~63	30~48	28~47	39~44
Number of Mice	27	17	22	35

For pharmacological studies, ECG was recorded continuously before administering the study drug and 5-10 minutes thereafter. Atropine (Sigma, #A0132) was dissolved in ethyl alcohol at 50 mg/ml and diluted to 1 mg/ml in PBS prior to IP injection at a dose of 1-2 μg/g. Isoproterenol (Sigma, #I5752) was dissolved in PBS at 1 mg/ml and diluted to 10 μg/ml prior to IP injection at a dose of 250 ng/g. ECGs are presented at baseline and 1 minute following drug administration. Metoprolol (Sigma #M5391) was dissolved in PBS at 200mg/ml and then diluted to 2mg/ml in PBS prior to IP injection at a final dose of 4μg/g. Diltiazem hydrochloride (Sigma #D2521) was dissolved in PBS at 200mg/ml and then diluted to 50mg/ml in PBS prior to IP injection at a final dose of 50μg/g. ECGs are presented at baseline and 5-10 minute following drug administration.

Based on ECG analysis of each mouse, the degree of AVB was labeled as follows: 1°, PR prolongation without dissociation from QRS complex; 2°, partial dissociation between P wave and QRS complex as evidenced by intermittent absence of QRS complex following a P wave with our without progressive PR prolongation; 3° AVB, complete dissociation between P wave and QRS complex most commonly evidenced by distinct PP and RR intervals. When 3° AVB was observed in juvenile and adult mice, it was always permanent. For the majority of neonatal animals, 3° AVB was permanent. However, in a subset of neonatal iAVB mice that showed evidence of recovery, 3° AVB was temporary. 3° AVB was confirmed on separate recordings at other time points for each mouse.

Data Analysis and Statistical Considerations. For all studies involving cohorts of mice, entire litters were characterized as a group with consistent analytical time points across litters. Only mice that survived tamoxifen induction were included in cohort analysis. However, certain iAVB and littermate control mice were sacrificed at pre-specified time points for histological analysis (Figures 1D, 1F, and 3F), while others died spontaneously following tamoxifen induction (see Figures 2B, S6, and S9B). Therefore, all animals for which data was available were included in the studies represented by Figures 2C-G, 3C-E, and S9C. For the data shown in Figure 3C, only mice that had serial ECGs from the time of tamoxifen induction until at least 1 month post-injury were included in the analysis. Recovery was adjudicated for iAVB mice if and only if there was ECG evidence of AVCS injury (i.e. 1°, 2°, or 3° AVB) prior to improvement in cardiac rhythm. Although we observed 3 additional neonatal iAVB mice with normal sinus rhythm at P28 (data not shown), these animals were excluded from our analysis since ECG evidence of prior AVCS injury was not obtained. For Figure 2G, all mice for which echocardiography data was available at P63 were included. This time point was chosen to minimize the contribution of compensatory mechanisms yet maximize capture at the terminal rhythm (see Figure 2E). All data are shown as mean ± s.e.m. P values were determined using the Fisher's Exact Test (Figure 3C), Log Rank statistical test (Figures 2B, S6, and S9B), or Student's two-tailed t-test (Figures 2C-D and F-G). A p value less than 0.05 was considered to be statistically significant. In figure panels

throughout the manuscript, the following labeling conventions for statistical testing are used: ns, $p > 0.05$;

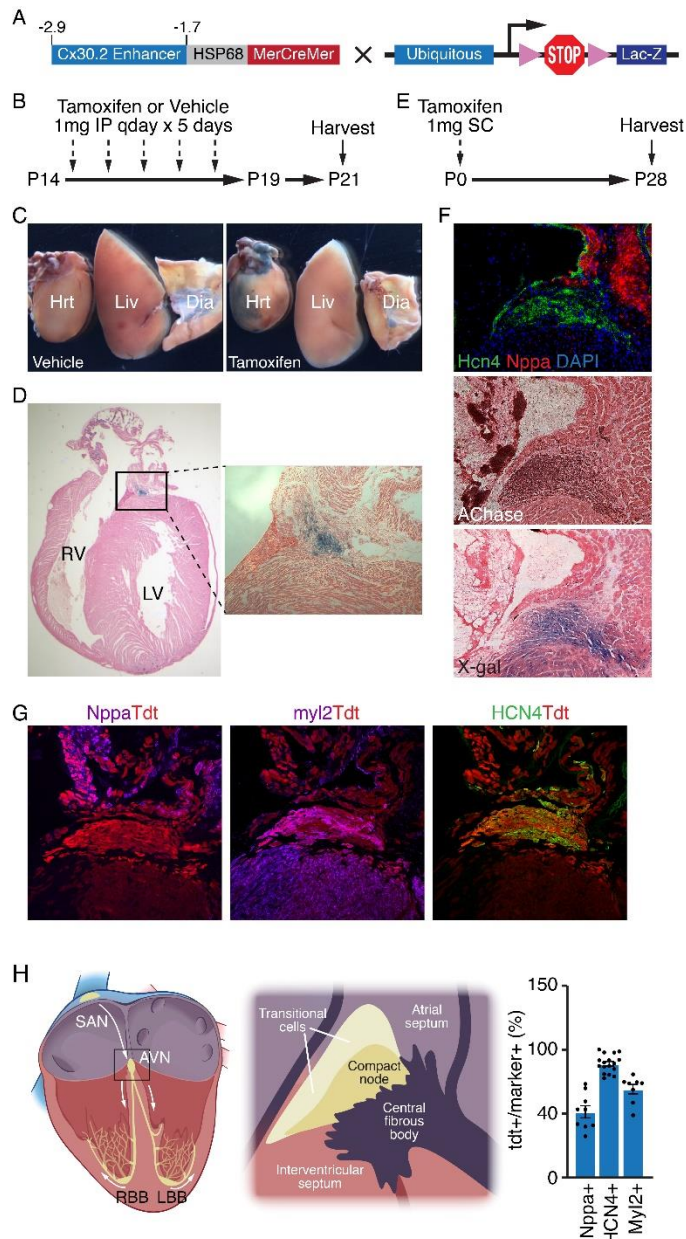*, $p < 0.05$; **, $p < 0.01$; ***, $p < 0.001$; ****, $p < 0.0001$.

Figure S1. Precise and inducible recombination within the AVCS. A) Strategy for evaluating spatiotemporal regulation of Cre recombinase activity in Tg(Cx30.2-MerCreMer) mice. B) Juvenile tamoxifen induction protocol. C) X-gal-stained whole-mount heart (Hrt), liver (Liv), and diaphragm (Dia) from vehicle- or tamoxifen-treated Tg(Cx30.2-MerCreMer)/+; Rosa26$^{LacZ/+}$ mice harvested at P21. X-gal staining was only observed in the heart following tamoxifen induction. X-gal$^+$ cells were seen in the right atrium and left ventricle as noted previously(11). D) Histological section of the X-gal$^+$ heart in (C) demonstrating anatomical localization of Cre activity to the AVCS. E) Neonatal tamoxifen induction protocol. F) Immunostaining analysis of a P28 Tg(Cx30.2-MerCreMer)/+; Rosa26$^{LacZ/+}$ mouse heart following tamoxifen induction. Consecutive sections were stained for Hcn4 (AVCS marker) and Nppa (atrial marker), acetylcholinesterase (AChase; AVCS marker) activity, and X-gal (LacZ marker). G) Same as in (F) using a P28 Tg(Cx30.2-MerCreMer)/+; Rosa26$^{tdTomato/+}$ mouse. Consecutive sections were stained for Nppa, Myl2, and Hcn4. Bar graph shows quantification of Tdtomato$^+$/marker$^+$ cells. H) Schematic depiction of the CCS (left) with a zoomed view of the AVCS (right). N=3.
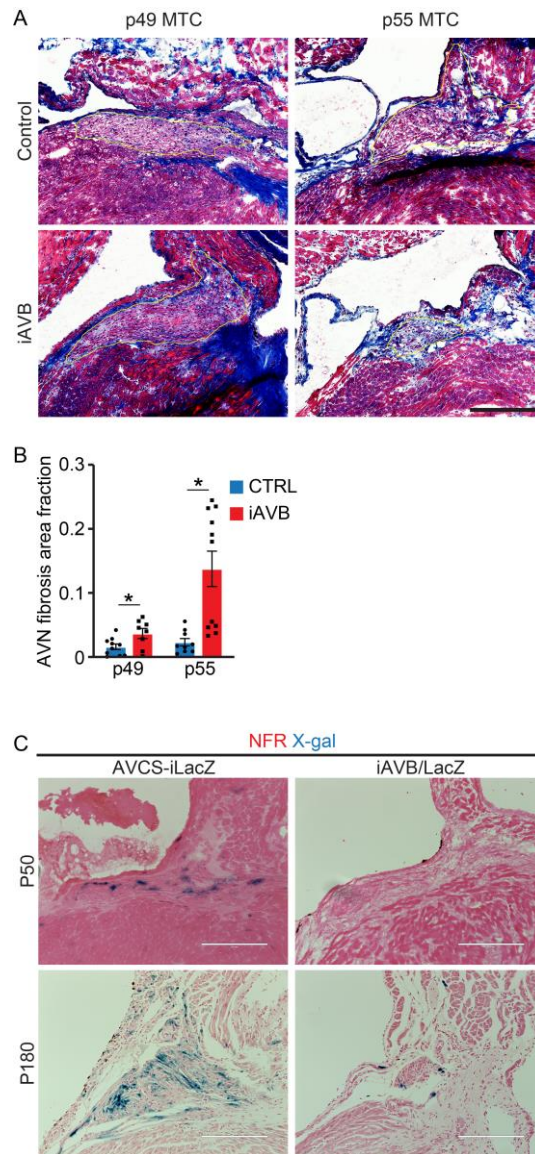
Figure S2. Fibrosis and loss of X-gal⁺ AVCS cells in adult iAVB mice. A) The hearts of iAVB and control mice were cryosectioned at P49 or P55 and stained with Masson's Trichrome (MTC; fibrosis marker). A representative tracing is shown (N=3). Scale bar, 200μm. B) Fibrotic area was quantified as a fraction of total AVN area (N=3). C) Tg(Cx30.2-MerCreMer)/+; Rosa26$^{LacZ/+}$ (AVCS-iLacZ) and Tg(Cx30.2-MerCreMer)/+; Rosa26$^{DTA/LacZ}$ (iAVB) mice were sacrificed at P50 (top) or P180 (bottom) and stained for lacZ activity. X-gal⁺ AVCS cells were reduced in adult iAVB mice compared with AVCS-iLacZ animals at both time points. N=3 (P50); N=1 (P180). Scale bar, 200μm. Mean values are shown with error bars representing s.e.m. *, p<0.05.
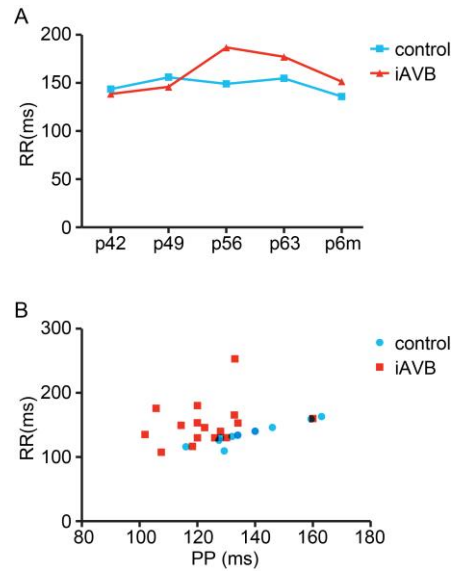
Figure S3. RR interval and PP-RR interval correlation in adult iAVB mice. A) RR intervals were measured in Rosa26$^{DTA/LacZ}$ (control) and Tg(Cx30.2-MerCreMer)/+; Rosa26$^{DTA/LacZ}$ (iAVB) mice at the indicated time points. B) Correlation plot of RR interval versus PP interval, demonstrating linear correlation in controls and scattered distribution in iAVB mice. N=28.
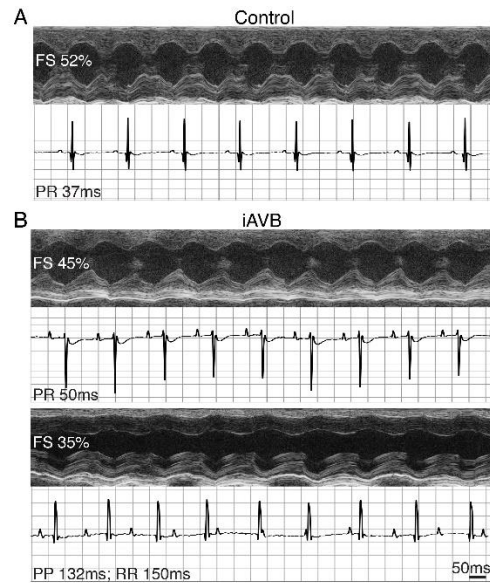
Figure S4. Contractile dysfunction correlates with severity of AV block in adult iAVB mice. A) Representative M-mode and ECG tracing from a control mouse in NSR (N=28). B) Representative M-mode and ECG tracings from iAVB mice with 1^O AVB (top) or 3° AVB (bottom). FS and relevant ECG intervals for each animal are shown in the associated tracings (N=28).
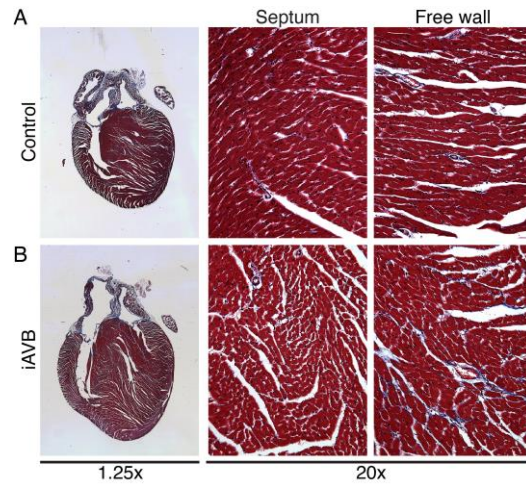
Figure S5. Histology of ventricular myocardium in adult iAVB mice. A) Control and B) 3° iAVB mouse hearts were sectioned at P180 and stained with MTC to visualize left ventricular fibrosis and scarring (N=3).
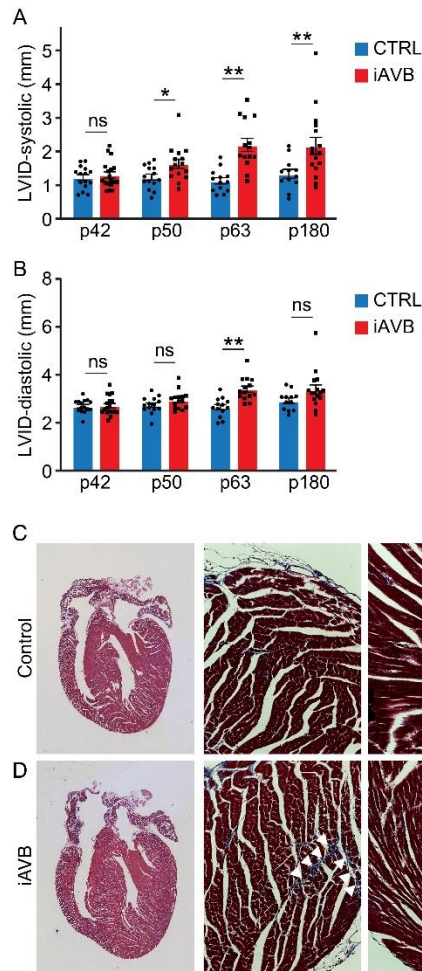
Figure S6. Ventricular chamber remodeling and interstitial fibrosis in adult iAVB mice. A) Left ventricular internal diameter during systole (LVID-S) was quantified in Rosa26[DTA/LacZ] (control) and Tg(Cx30.2-MerCreMer)/+; Rosa26[DTA/LacZ] (iAVB) mice. B) Left ventricular internal diameter during diastole (LVID-D) was quantified in control and iAVB mice. C) Histological section of control and iAVB mice at P180 demonstrating evidence of interstitial fibrosis (white arrowheads) in the iAVB heart. ns, non-signficant; *, p<0.05; **, p<0.01. N=28. Scale bar, 200μm.
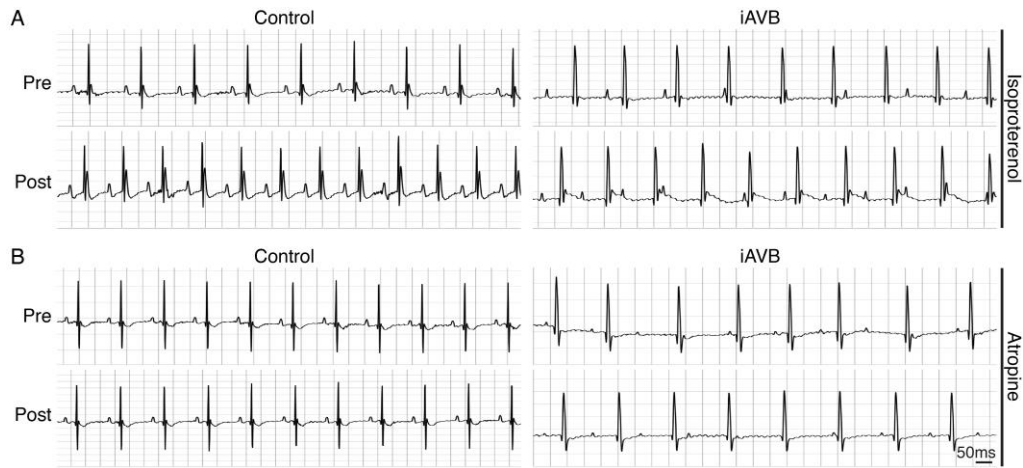
Figure S7. Pharmacological responses in adult iAVB mice. A) An adult iAVB mouse demonstrating persistent 3° AVB (right) and a littermate control (left) in NSR were injected with isoproterenol, and ECGs were recorded (N=10). B) Similar experimental setup as in (A) was used to evaluate the effect of atropine (N=10).
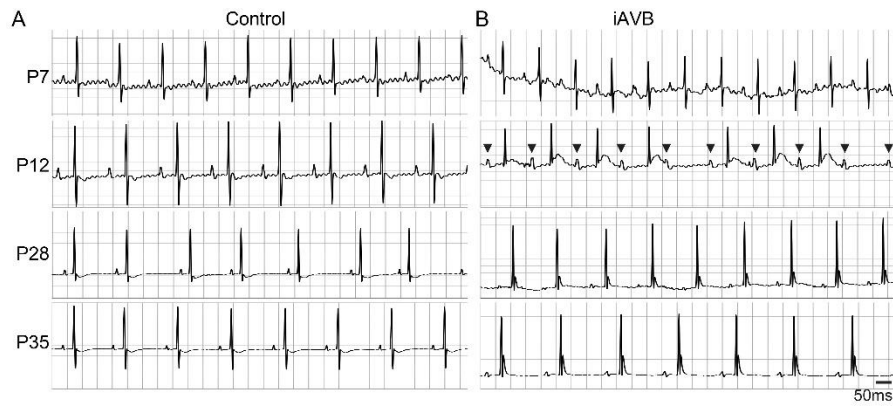
Figure S8. Serial ECG analysis reveals potential regenerative capacity of neonatal iAVB mice.
A-B) Following tamoxifen induction at P0, serial ECG tracings were obtained at P7, P12, P28, and
P35 for an iAVB mouse and littermate control. Representative tracings are shown (N=42). Solid
arrowheads indicate P waves.
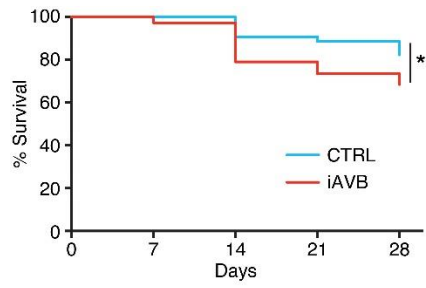
Figure S9. Survival analysis in neonatal mice following AVCS ablation. Kaplan-Meier plot of neonatal Rosa26^DTA/LacZ (control) and Tg(Cx30.2-MerCreMer)/+; Rosa26^DTA/LacZ (iAVB) mice for 1 month post-injury is shown. *, p<0.05. N=160.

Figure S10. Example of recovery from 3° AVB following neonatal AVCS injury. Serial ECGs obtained from a neonatal Tg(Cx30.2-MerCreMer)/+; Rosa26$^{DTA/LacZ}$ (iAVB) mouse with evidence of recovery from 3° AVB. N=42.
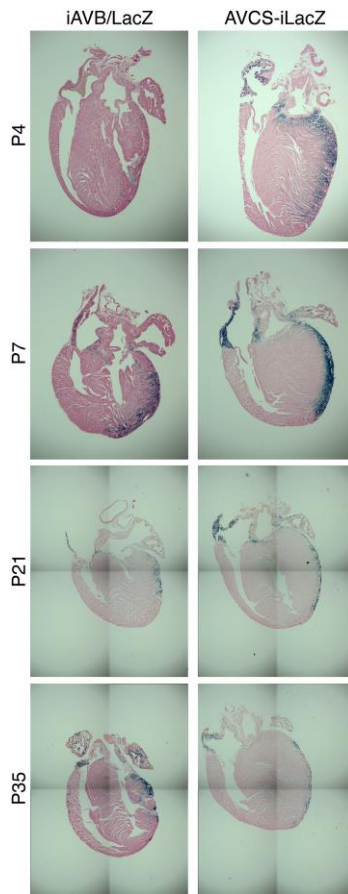
Figure S11. Whole-heart images for Figure 3D. Whole-heart images were obtained following X-gal staining in Tg(Cx30.2-MerCreMer)/+; Rosa26$^{DTA/LacZ}$ (iAVB) and Tg(Cx30.2-MerCreMer)/+; Rosa26$^{LacZ/+}$ (AVCS-iLacZ) mice at the indicated time points. Images correspond to those shown in Figure 3D. Scale bar, 1000μm.
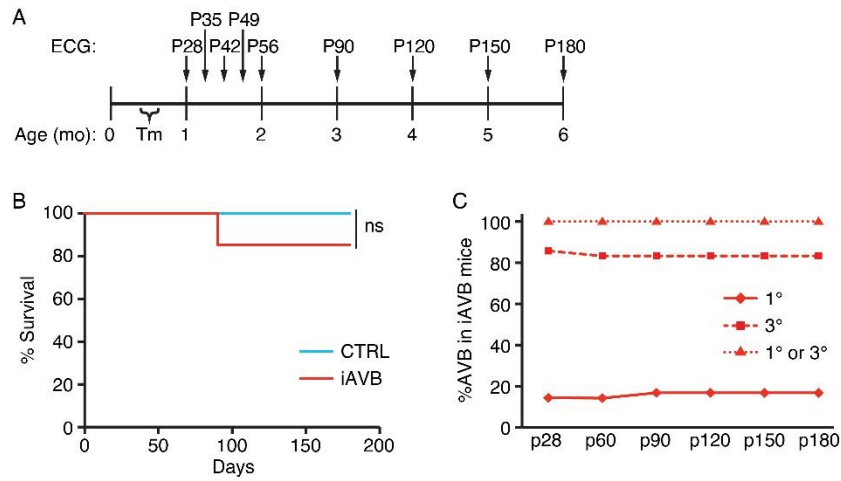
Figure S12. Survival and cardiac rhythm analysis in juvenile mice subjected to AVCS injury.
A) Schedule of ECG acquisition for longitudinal analysis of juvenile Rosa26$^{DTA/LacZ}$ (control) and Tg(Cx30.2-MerCreMer)/+; Rosa26$^{DTA/LacZ}$ (iAVB) mice.   B) Kaplan-Meier plot of iAVB vs. control mice shows no significant survival difference between the two groups. C) Plot of the predominant rhythm versus time in juvenile iAVB mice demonstrates no evidence of recovery from AVCS injury. ns, non-signficant. N=10.
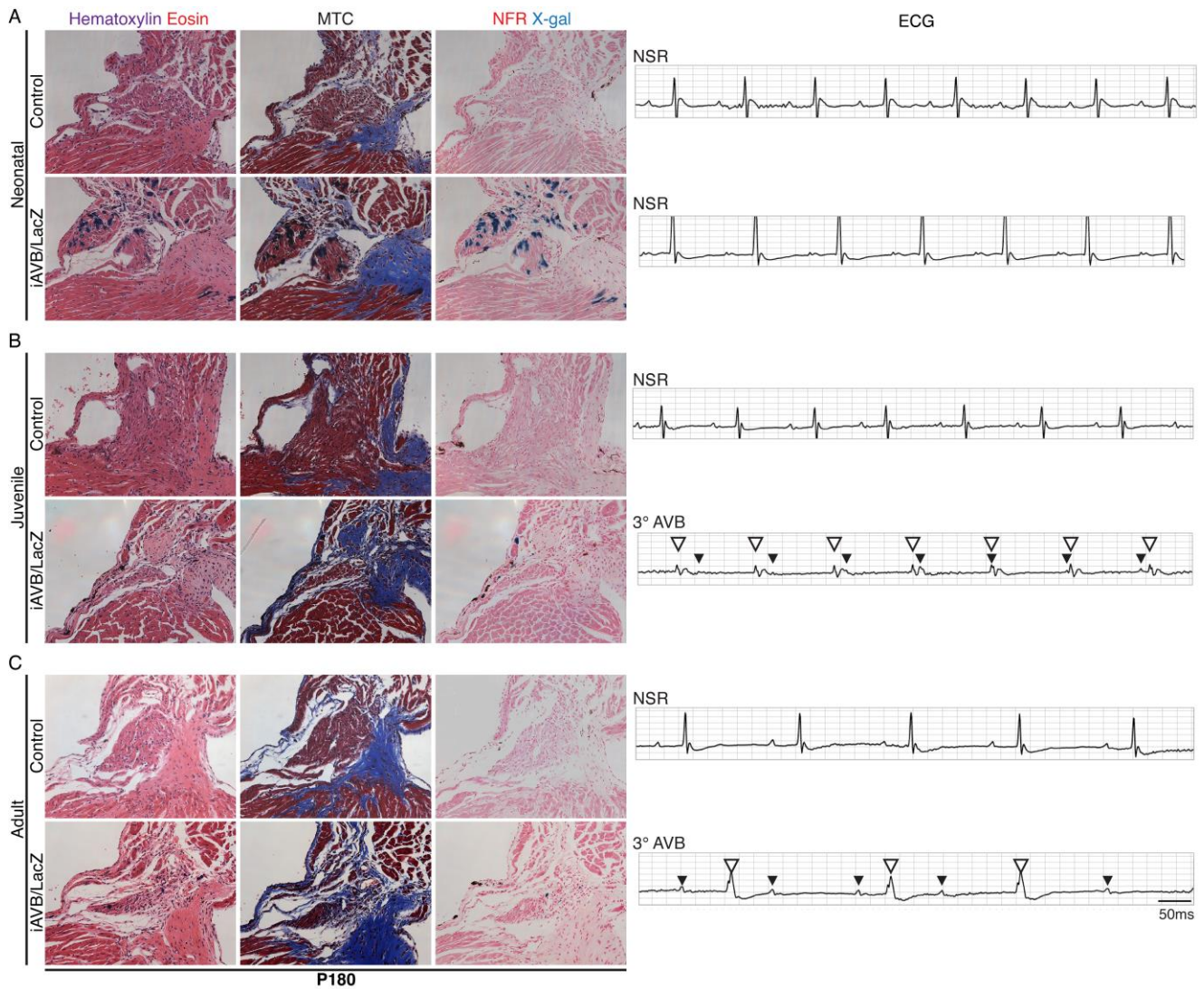
Figure S13. Recovery from dysrhythmia is durable. Tissue sections were collected at P180 from Tg(Cx30.2-MerCreMer)/+; Rosa26$^{DTA/LacZ}$ (iAVB) mice and littermate controls for A) neonatal, B) juvenile, and C) adult iAVB mice. Histological analysis is shown for H&E, MTC, and X-gal/NFR staining of matched sections (left panels) along with the ECG (right panels) of corresponding mice prior to sacrifice. A) At 6 months following neonatal AVCS injury, recovery of NSR was evident in the iAVB mouse with minimal AVCS architectural disruption and abundant X-gal$^+$ cells. B) iAVB mice that underwent juvenile AVCS injury remained in 3° AVB with concomitant AVCS fibrosis and architectural disruption in the absence of significant X-gal$^+$ cells. C) Adult iAVB mice displayed similar characteristics to juvenile iAVB mice but with greater AVCS architectural disruption and fibrotic replacement, similar to what is seen in humans with acquired CHB. N=18.
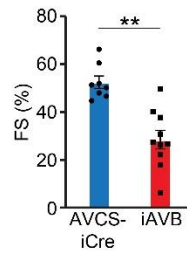
Figures S14. Ventricular function in neonatal iAVB mice. Tg(Cx30.2-MerCreMer)/+; Rosa26^DTA/tdTomato (iAVB) and Tg(Cx30.2-MerCreMer)/+; Rosa26^tdTomato/+ (AVCS-iCre) mice were injected with tamoxifen at P0 and aged until P180. Echocardiograms were performed, and quantification of fractional shortening (FS) demonstrated a reduction in neonatal iAVB mice. **, p<0.01. N=18.
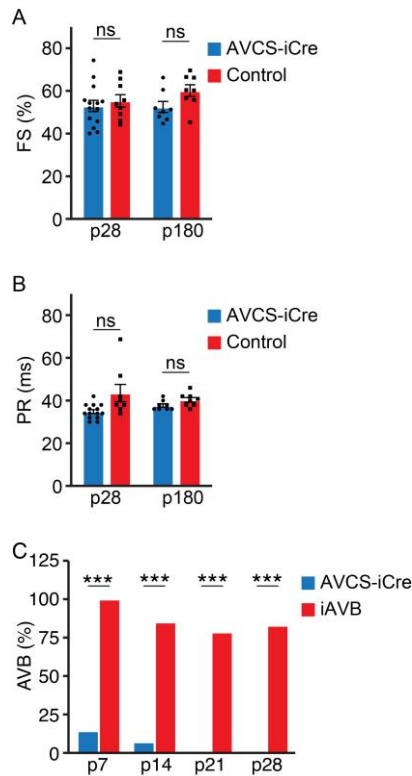
Figures S15. Neonatal Cre induction does not cause significant cardiac dysfunction. A) Bar graph showing fractional shortening (FS) in Tg(Cx30.2-MerCreMer)/+; Rosa26$^{tdTomato/+}$ (AVCS-iCre) and Rosa26$^{DTA/LacZ}$ (control) mice at P28 and P180. No significant differences were observed. B) Bar graph showing PR interval in AVCS-iCre and control mice at P28 and P180. No significant differences were observed. C) Bar graph showing the percentage of mice with atrioventricular block (AVB) up to 1 month of age in AVCS-iCre and Tg(Cx30.2-MerCreMer)/+; Rosa26$^{DTA/LacZ}$ (iAVB) mice. AVCS-iCre mice did not display significant AVB as compared to neonatal iAVB mice. ns, non-signficant; ***, $p<0.001$. N=16.
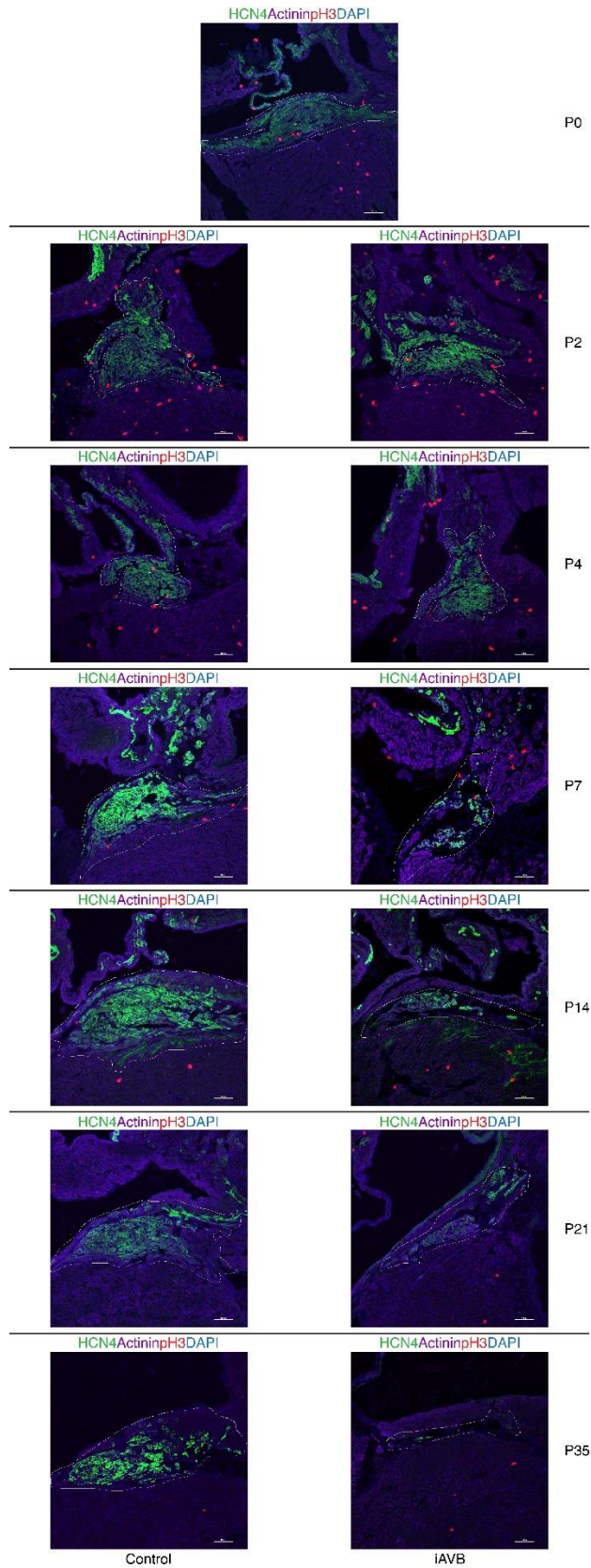
Figure S16. Representative sections from control and injured mice following neonatal tamoxifen induction. Example micrographs from heart sections collected from control and injured iAVB mice and stained with Hcn4, α-actinin, pH3, and DAPI. Quantification was conducted as detailed in Methods. N=3. Scale bar, 100mm.
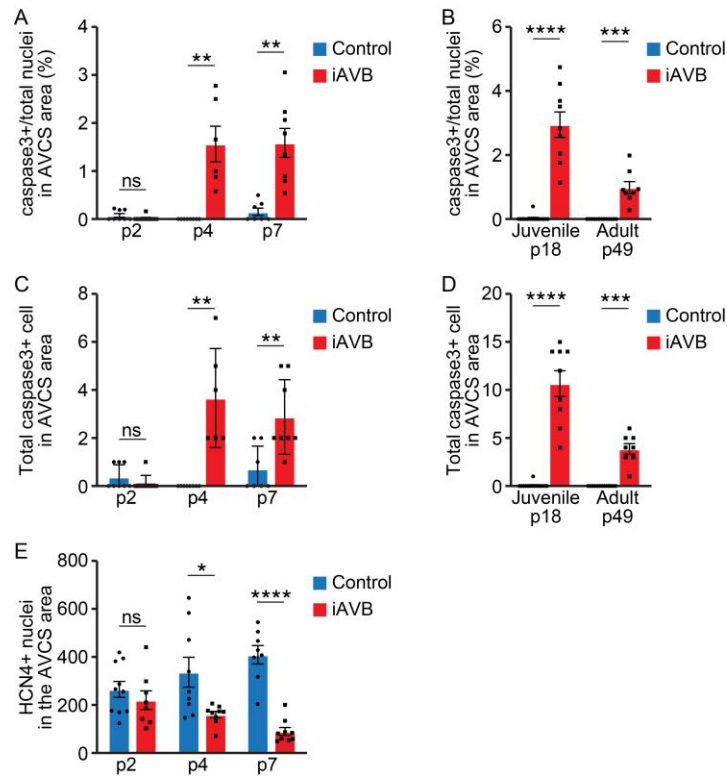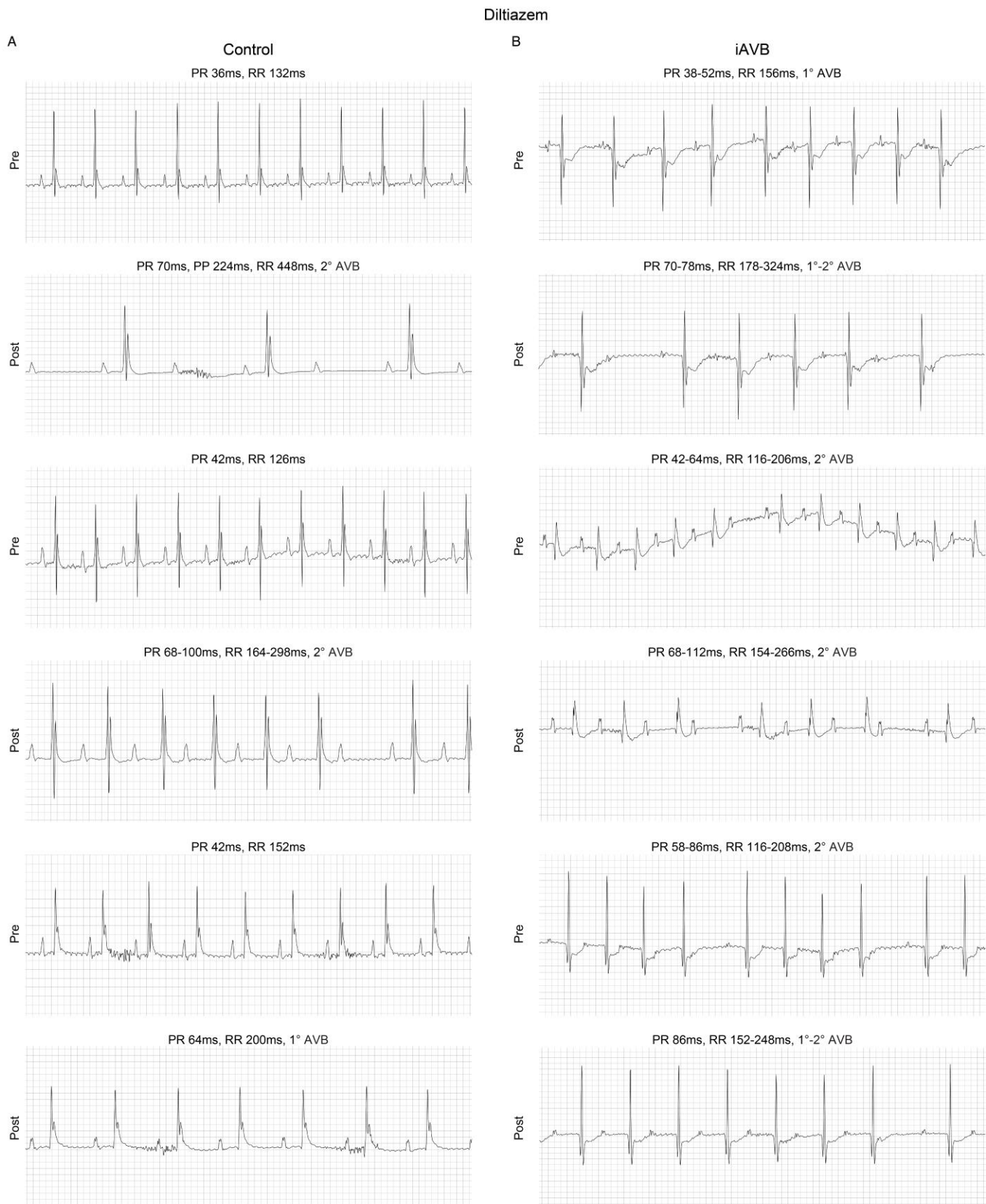
Figure S17. Quantification of cell death and conduction cells in iAVB mice. A) Activated caspase 3 staining was performed in Rosa26$^{DTA/LacZ}$ (control) and neonatal Tg(Cx30.2-MerCreMer)/+; Rosa26$^{DTA/LacZ}$ (iAVB) mice at P2, P4, and P7. Bar plot shows the percentage of caspase3$^+$ cells in the AVCS. B) Same as in (A) showing the percentage of caspase3$^+$ cells in the AVCS of juvenile and adult iAVB mice. C) Absolute number of caspase3$^+$ cells in the AVCS of neonatal iAVB mice. D) Absolute number of caspase3$^+$ cells in the AVCS of juvenile and adult iAVB mice. E) Absolute number of Hcn4$^+$ AVCS cell nuclei in control and neonatal iAVB mice at P2, P4, and P7. ns, non-significant; *, p<0.05; **, p<0.01; ***, p<0.001; ****, p<0.0001. N=6.
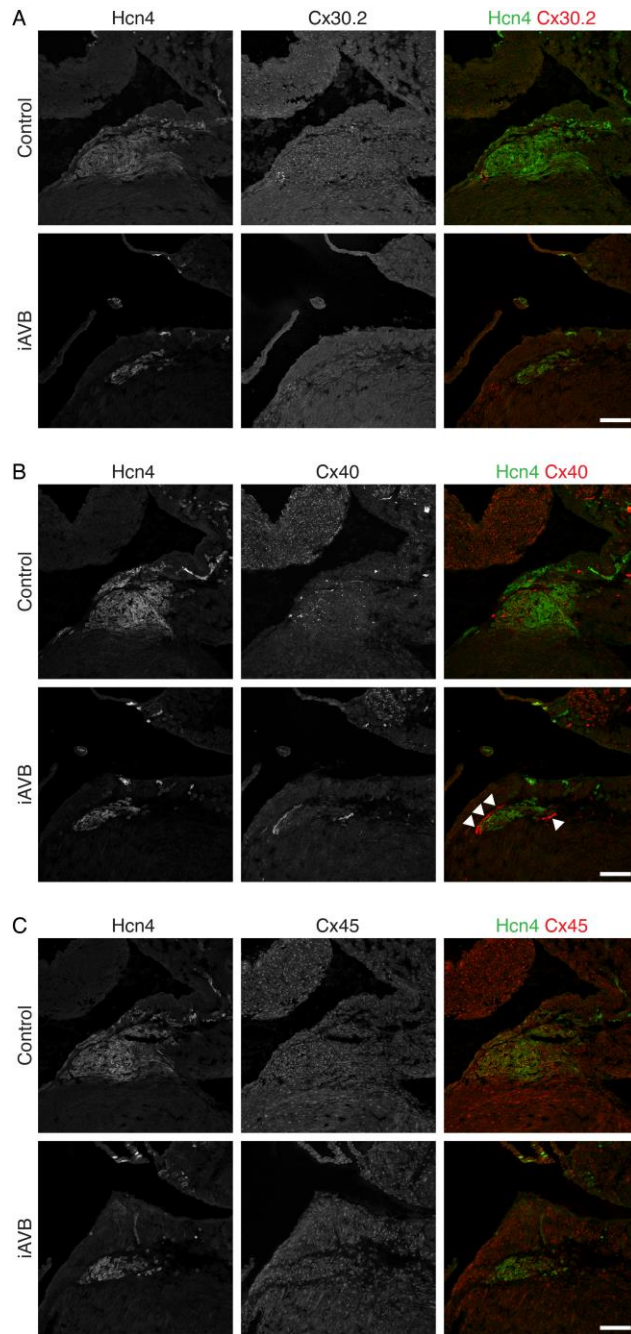
Figures S18. Connexin distribution in neonatal iAVB mice. A) Rosa26$^{DTA/LacZ}$ (control) and recovered neonatal Tg(Cx30.2-MerCreMer)/+; Rosa26$^{DTA/LacZ}$ (iAVB) mice were sacrificed at P21 and sectioned for Cx30.2 and Hcn4 immunostaining. Cx30.2 expression is reduced in the iAVB heart compared with control. B) Same as in (A) and stained for Cx40. A linear rim of Cx40^{+}/Hcn4^{-} cells (white arrowheads) is evident above and below the Hcn4^{+} AVCS in the iAVB heart as compared to the sparse Cx40 expression observed in the control heart. C) Same as in (A) and stained for Cx45. Expression of Cx45 is unchanged in the iAVB heart compared to the control. N=6. Scale bar, 100μm.
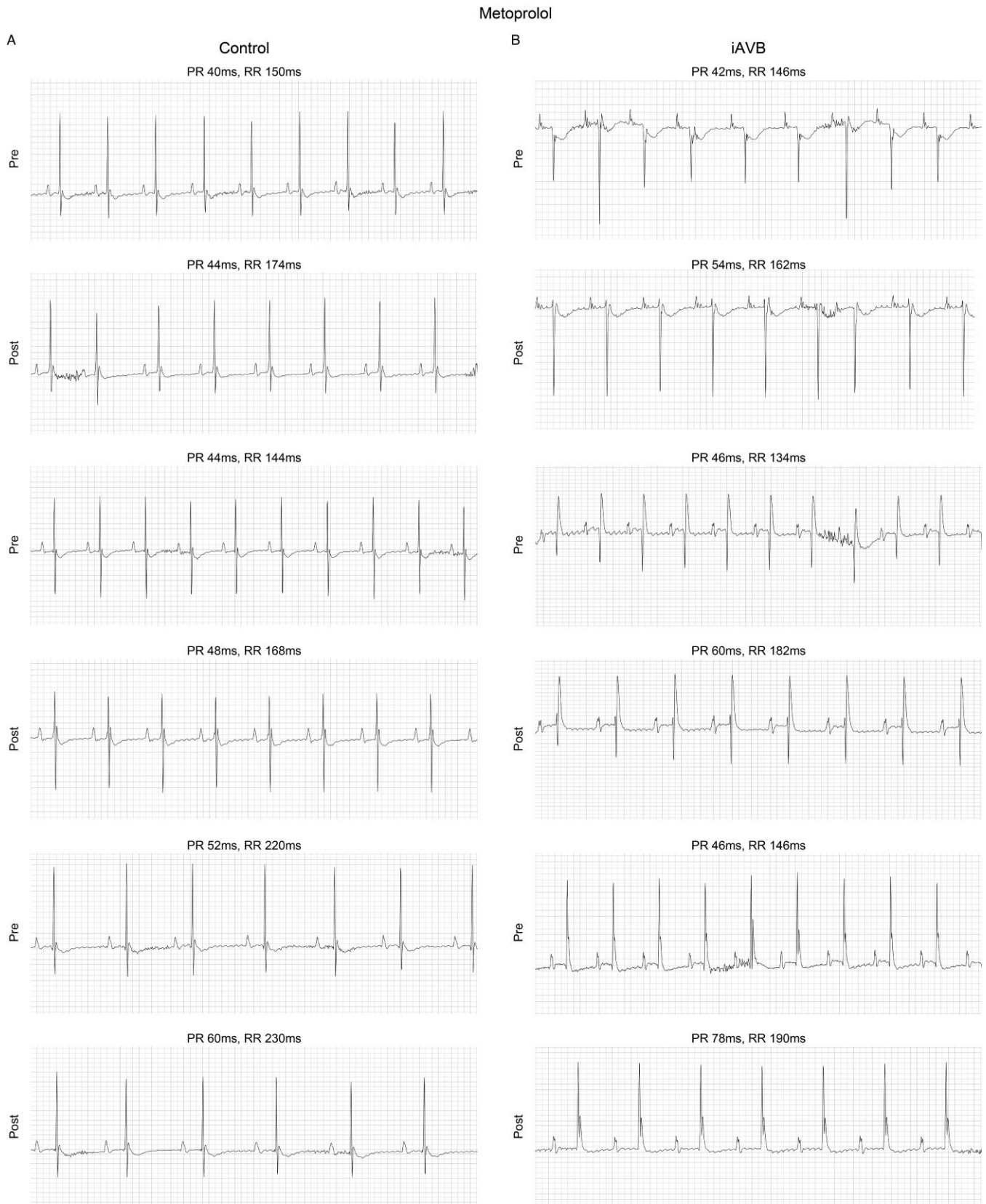
Figures S19. Cardiac electrical effects of acute metoprolol administration in recovered neonatal iAVB mice. A) Rosa26$^{DTA/LacZ}$ (control) mice (N=3) were given intraperitoneal (IP) metoprolol, and ECGs were recorded before and after pharmacological stimulation. PR and RR intervals are indicated. B) Same as in (A) except that recovered neonatal Tg(Cx30.2-MerCreMer)/+; Rosa26$^{DTA/LacZ}$ (iAVB) mice (N=3) were analyzed.

Diltiazem

A Control

PR 36ms, RR 132ms

PR 70ms, PP 224ms, RR 448ms, 2° AVB

PR 42ms, RR 126ms

PR 68-100ms, RR 164-298ms, 2° AVB

PR 42ms, RR 152ms

PR 64ms, RR 200ms, 1° AVB

B iAVB

PR 38-52ms, RR 156ms, 1° AVB

PR 70-78ms, RR 178-324ms, 1°-2° AVB

PR 42-64ms, RR 116-206ms, 2° AVB

PR 68-112ms, RR 154-266ms, 2° AVB

PR 58-86ms, RR 116-208ms, 2° AVB

PR 86ms, RR 152-248ms, 1°-2° AVB

Figures S20. Cardiac electrical effects of acute diltiazem administration in recovered neonatal iAVB mice. A) Rosa26$^{DTA/LacZ}$ (control) mice (N=3) were given intraperitoneal (IP) diltiazem, and ECGs were recorded before and after pharmacological stimulation. PR and RR intervals are indicated along with degree of AVB. B) Same as in (A) except that recovered neonatal Tg(Cx30.2-MerCreMer)/+; Rosa26$^{DTA/LacZ}$ (iAVB) mice (N=3) were analyzed.
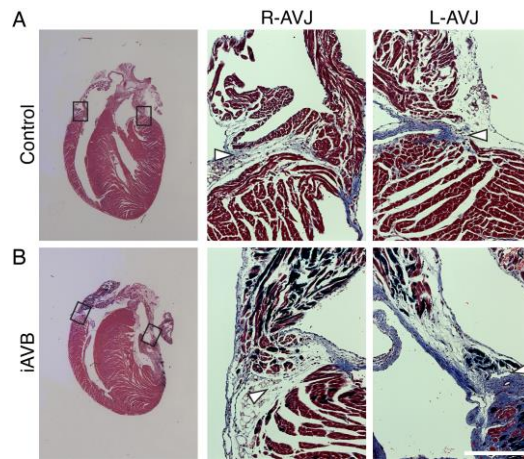
Figure S21. Lack of atrioventricular bypass tracts in a neonatal iAVB mouse. A) A P180 Rosa26$^{DTA/LacZ}$ (control) mouse heart was stained with Masson's Trichrome. Whole-heart (left) and zoomed (right) images are shown. B) Same as in (A) for a recovered neonatal Tg(Cx30.2-MerCreMer)/+; Rosa26$^{DTA/LacZ}$ (iAVB) mouse. No obvious muscular atrioventricular (AV) connections were observed in either heart. Black outlined arrowheads indicate the annulus fibrosus separating atria and ventricles. R-AVJ, right AV junction; L-AVJ, left AV junction. N=6. Scale bar, 200μm.
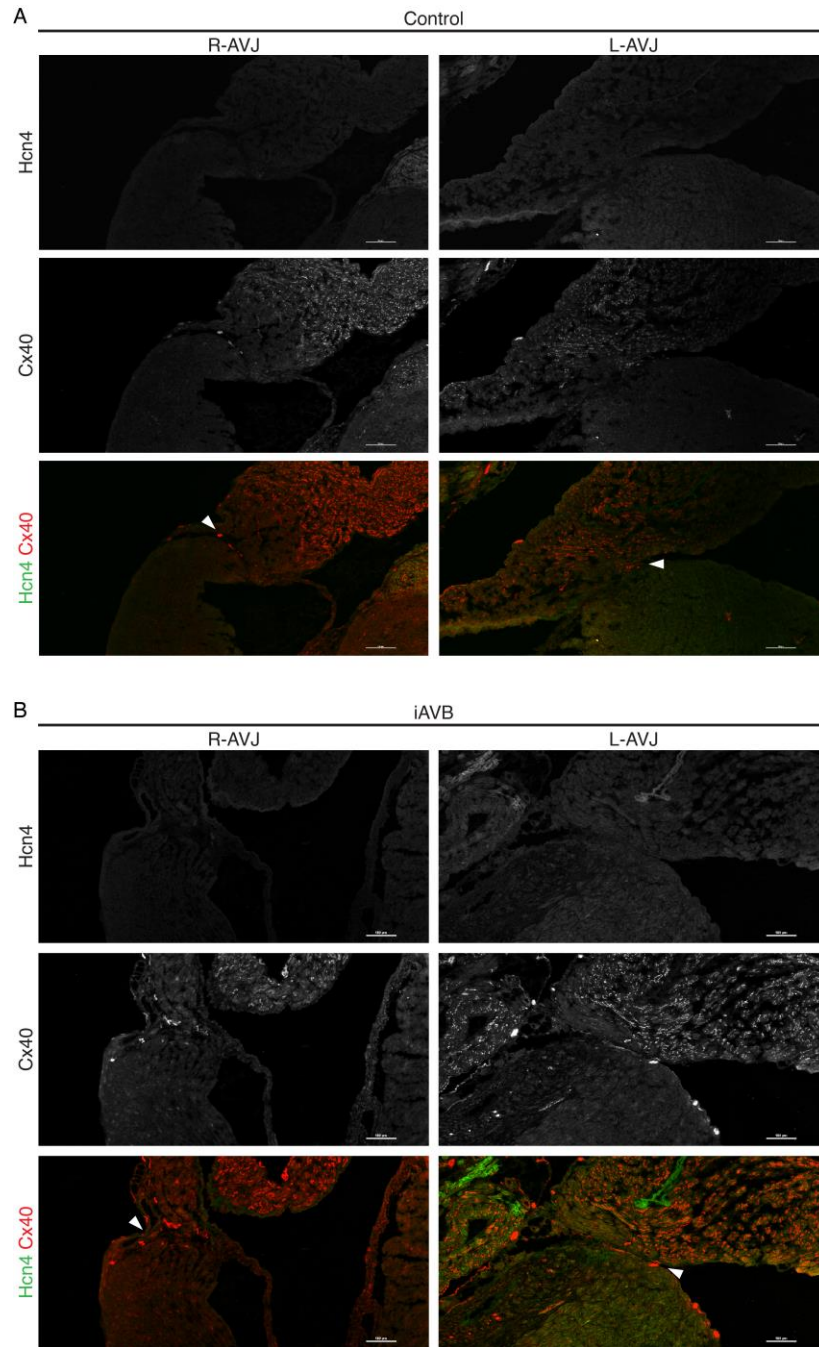
Figure S22. Lack of ectopic conduction tissue in a neonatal iAVB mouse. A) A P180 Rosa26$^{DTA/LacZ}$ (control) mouse heart was immunostained for Hcn4 and Cx40 to identify ectopic conduction tissue. B) Same as in (A) for a recovered neonatal Tg(Cx30.2-MerCreMer)/+; Rosa26$^{DTA/LacZ}$ (iAVB) mouse. No obvious ectopic conduction tissue was identified in either heart. White arrowheads highlight the transition between the atria and ventricles. R-AVJ, right AV junction; L-AVJ, left AV junction. N=6. Scale bar, 100μm.

Supplementary References

34. Hsieh PC, et al. Evidence from a genetic fate-mapping study that stem cells refresh adult mammalian cardiomyocytes after injury. *Nat Med.* 2007;13(8):970-4.
35. Arnolds DE, Moskowitz IP. Inducible recombination in the cardiac conduction system of minK: CreERT(2) BAC transgenic mice. *Genesis.* 2011;49(11):878-84.
36. El-Badawi A, Schenk EA. Histochemical methods for separate, consecutive and simultaneous demonstration of acetylcholinesterase and norepinephrine in cryostat sections. *J Histochem Cytochem.* 1967;15(10):580-8.